

Efficient Fabrication of Stable Graphene-Molecule-Graphene Single-Molecule Junctions at Room Temperature

Hantao Sun,^[a] Zhuoling Jiang,^[a] Na Xin,^[b] Xuefeng Guo,^[b] Shimin Hou,^{*,[a]} and Jianhui Liao^{*,[a]}

We present a robust approach to fabricate stable single-molecule junctions at room temperature using single-layer graphene as nanoelectrodes. Molecular scale nano-gaps in graphene were generated using an optimized fast-speed feedback-controlled electroburning process. This process shortened the time for creating a single nano-gap to be less than one minute while keeping a yield higher than 97%. To precisely control the gap position and minimize the effects of edge defects and the quantum confinement, extra-narrow grooves were pre-patterned in the graphene structures with oxygen plasma etching. Molecular junctions were formed by bridging the nano-gaps with amino-functionalized hexaphenyl molecules

by taking advantage of chemical reactions between the amino groups at the two ends of the molecules and the carboxyl groups at the edges of graphene electrodes. Electronic transport measurements and transition voltage spectroscopy analysis verified the formation of single-molecule devices. First-principles quantum transport calculations show that the highest occupied molecular orbital of hexaphenyl is closer to the Fermi level of the graphene electrodes and thus the devices exhibit a hole-type transport characteristics. Some of these molecular devices remained stable up to four weeks, highlighting the potential of graphene nano-electrodes in the fabrication of stable single-molecule devices at room temperature.

1. Introduction

Single-molecule devices, in which individual molecules are utilized as active electronic components, have blossomed into a powerful platform for exploring novel phenomena at the molecular scale and paving the way for electronic devices downscaling to the single-molecule level.^[1–3] Much progress has been made in the past decades. On the one hand, many methods have been developed to create nanometer-spaced electrodes, such as break junctions^[4,5] and scanning probe techniques.^[6,7] On the other hand, a wide range of characteristic functions were demonstrated in single-molecule devices including rectifiers^[8,9], transistors^[10–12], chemosensors^[13,14] and switches^[15,16]. Moreover, various fundamental physical phenomena beyond conventional electronic transport properties have been observed, such as quantum interference, electromechanic, thermoelectronic, optoelectronic and spintronic effects.^[17–20] Despite these successful achievements, there are still some general challenges remaining in single-molecule devices. One

of these challenges is the room-temperature stability, which is required for practical applications. In experiments, gold is the most preferred electrode material in metal-molecule-metal junctions, because gold is chemically inert under ambient conditions and many anchor groups can bond to the gold surface. However, the high mobility of surface atoms of gold at room temperature leads to the instability of the molecule-gold bond in ambient conditions.^[17–22] Alternatively, graphene has demonstrated as one of the most promising electrode materials for stable single-molecule devices at room temperature due to the following advantages.^[23–25] Firstly, atoms in graphene are stable at room temperature owing to their strong sp^2 C–C covalent bonds. Even the nano-gaps are formed at room temperature, the graphene electrodes will be stable for a long time. This enables us to generate nano-gaps in graphene structures firstly and interlink the electrodes using molecules subsequently. In this way, the risk of decomposing the molecules due to the local high temperature during the generation process of nano-gaps can be avoided.^[26,27] In addition, the electronic transport properties of the junctions before and after molecule connection can be directly compared to make sure the successful molecular connections. Secondly, the atomic thickness of graphene may result in least screening of an applied gate-field and thus enhances the gate coupling in three-terminal devices.

Several groups have reported the fabrication of molecular devices using few-layer or single-layer graphene (SLG) as electrodes.^[23,27–39] Two distinct experimental approaches have been demonstrated to construct graphene nano-gaps, i.e. the dash-line lithographic plasma etching and the feedback-controlled electroburning.^[28,23,27,30] The former is the local cutting of graphene using oxygen plasma etching in an array of

[a] H. Sun, Z. Jiang, S. Hou, J. Liao
Centre for Nanoscale Science and Technology, Key Laboratory for the Physics and Chemistry of Nanodevices, Department of Electronics,
Peking University
Beijing 100871, China
E-mail: smhou@pku.edu.cn
Jianhui.Liao@pku.edu.cn

[b] N. Xin, X. Guo
Beijing National Laboratory for Molecular Sciences, State Key Laboratory for Structural Chemistry of Unstable and Stable Species, College of Chemistry and Molecular Engineering,
Peking University,
Beijing 100871, China

Supporting information for this article is available on the WWW under <https://doi.org/10.1002/cphc.201800220>

holes formed with dashed line e-beam lithography in PMMA layer. The latter is Joule heating induced break-down of graphene in the presence of oxygen, and the process evolution is controllably performed using a feedback control system. Despite these inspiring progresses, challenges still exist in the fabrication of graphene nano-electrodes. One challenge is the complexity and the corresponding low yield of device fabrication. For the electroburning method, when employed with pre-patterning, this technique can have a precise control over the gap size and position while keeping a high yield up to 95%.^[27,31] Another challenge is the consuming time during the electroburning process. Although the application of SLG allows to fabricate junctions in large arrays, the present feedback-controlled electroburning process will cost a lot of time. Furthermore, the influence of edge defects and the quantum confinement effects might become more and more nonnegligible with the narrowing of graphene and formation of nano-gaps.^[40] However, these issues have rarely been considered comprehensively up to now.

Here we report a robust approach to fabricate stable molecular junctions at room temperature using SLG as the nano-electrodes that were grown by chemical vapor deposition (CVD) on Cu and then transferred to silicon substrate. We optimized the initial device structure as well as the feedback-controlled electroburning process to achieve a high efficiency and a high yield. Amino-terminated hexaphenyl aromatic molecules (4,4'-diaminohexaphenyl, DAHP) were used to bridge the graphene nano-gaps. The current-voltage characteristics and room-temperature stability of the fabricated graphene-hexaphenyl-graphene (GHG) molecular devices were measured experimentally, and the conduction mechanism of these GHG molecular junctions was investigated by employing the non-equilibrium Green's function formalism combined with density functional theory (the NEGF + DFT approach).

Experimental Section

Device Fabrication

Photolithography and electron beam evaporation (5 nm Ti/40 nm Au) were used to define a grid of alignment marks with 500 μm pitches on the silicon wafer coated with 300 nm thermal silicon dioxide. The CVD-grown SLG was separated from the copper substrate using the electrolytic bubbling method and transferred to the silicon substrate with the alignment grid.^[41] An optical microscope (Carl Zeiss Axio Imager) was used to map the position of SLG flakes with respect to the alignment grid. Raman spectroscopy (LabRAM HR800, Jobin Yvon/Horiba company) was used to assess the quality of the SLG. Electron beam lithography (Raith 150II) was employed to pattern electrodes with channel lengths of 1 μm . Subsequently, metallic source/drain electrodes (5 nm Ti/45 nm Au) were deposited using the electron-beam evaporation. The electron beam lithography was used again to pattern windows in PMMA (A4 950k). The SLG between Ti/Au electrodes was etched into a notched ribbon with two extra-narrow (80 nm) grooves using oxygen plasma etching.

Fabrication of Nano-Gaps by the Electroburning Process

We used an optimized fast-speed feedback-controlled electroburning process to generate nano-gaps in graphene. The electroburning process was conducted in air at room temperature inside a probe station (Lakeshore TTP4). The process was controlled using a homemade LabVIEW program based on a data acquisition board (National Instruments, PCI 6281). A voltage ramp (1 V/s) was applied to the source-drain electrodes while recording the corresponding source-drain current continuously at a sampling rate of 50 KHz. The conductance measured at 0.1 V was set as the reference value. When the conductance was decreased by 5%, the applied bias was retracted by 20% immediately. The end conductance in the last cycle was used as the reference value for the next cycle. The voltage ramping cycles were repeated until a target resistance (500 M Ω –1 G Ω) was reached.

Formation of Molecular Junctions

For molecular connection, we used the method described in the literature.^[25] DAHP molecules were first dissolved in anhydrous pyridine (Alfa Aesar, 99.5%) with the concentration of 0.1 mM. Then the graphene devices and 1-(3-Dimethylaminopropyl)-3-ethylcarbodiimide hydrochloride (Alfa Aesar, 98%, EDCI) were added into the DAHP solution for connection for over 48 hours in dark. EDCI was used as a carbodiimide dehydrating/activating agent. To prevent the molecules from oxidation, the molecular connection process was performed in argon environment. After that, the devices were taken out from the solution and rinsed with acetone and ultrapure water. Finally, a N₂ gas stream was used to blow the devices dry.

Electronic Measurements

We recorded current-voltage (I - V) curves of GHG molecular devices in a vacuum probe station (LakeShore TTP4). The I - V curves were measured using a data acquisition board (National Instruments, PCI 6281) together with a homemade LabVIEW program. A low-noise current amplifier (Ithaco 1211) was used to convert current to voltage. All device measurements were performed in vacuum ($P < 1 \times 10^{-4}$ Torr) at room temperature. Devices were characterized by scanning electron microscope (SEM, Raith 150II) after electronic measurements.

Theoretical Calculations

We use the SIESTA code to compute the atomic structure of GHG molecular junctions and the quantum transport code SMEAGOL to study their electronic transport properties.^[42–45] SIESTA is an efficient DFT package, in which the atomic cores are described by improved Troullier-Martins pseudopotentials and the wave functions of the valence electrons are expanded with a finite-range numerical orbital basis set.^[42,46] We construct a double-zeta plus polarization basis set for the H, C, N and O atoms. The generalized gradient approximation within the Perdew-Burke-Ernzerhof formulation is used for the exchange-correlation functional.^[47] The interlayer distance of the graphene sheets is set to be 15 Å in order to model isolated two-dimensional graphene electrodes. After performing geometric optimization by conjugate gradient the residual forces acting on the atoms in the device region are smaller than 0.02 eVÅ⁻¹.

SMEAGOL is a practical implementation of the NEGF + DFT approach, which employs SIESTA as the DFT platform.^[43–45] The unit cell of the extended molecule comprises two graphene electrodes with zigzag edges passivated by hydrogen atoms and the

hexaphenyl molecule embedded between them. Here the transport is assumed to be along the z -axis and the graphene electrodes are placed in the y - z plane. We always consider periodic boundary condition along the y -axis, so that the graphene electrodes are infinite. The total transmission coefficient $T(E)$ of the junction is evaluated as

$$T(E) = \frac{1}{\Omega_{1\text{DBZ}}} \int_{1\text{DBZ}} T(\vec{k}, E) d\vec{k} \quad (1)$$

where $\Omega_{1\text{DBZ}}$ is the length of the one-dimensional Brillouin zone (1DBZ) along the y -axis. The k -dependent transmission coefficient $T(k, E)$ is obtained as

$$T(\vec{k}, E) = \text{Tr}[\Gamma_L G_M^R \Gamma_R G_M^{R+}] \quad (2)$$

Where G_M^R is the retarded Green's function matrix of the extended molecule and Γ_L (Γ_R) is the broadening function matrix describing the interaction of the extended molecule with the left-hand (right-hand) side electrode. Here, we calculate the transmission coefficient by sampling 8 k -points in the transverse 1DBZ.

2. Results and Discussion

To fabricate graphene electrodes, we started with CVD-grown SLG on a copper substrate. The whole process is schematically shown in Figure 1. The SLG was transferred from the copper

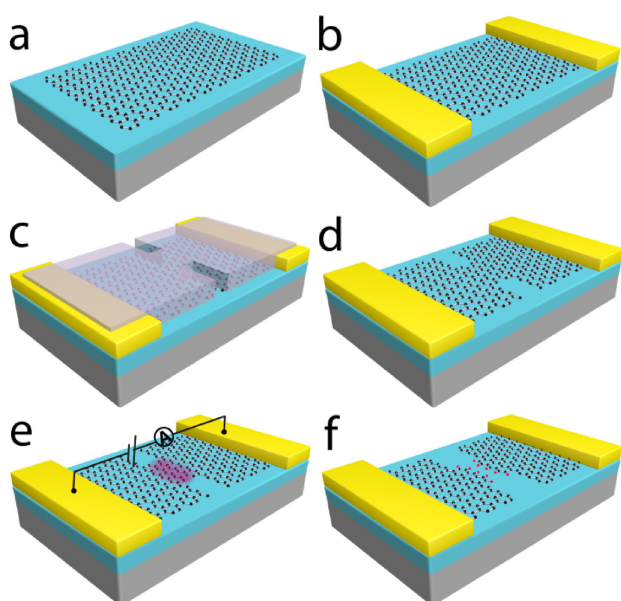


Figure 1. Schematics for the fabricating process of nano-gaps in single-layer graphene (SLG). (a) SLG was transferred to a degenerately doped silicon substrate coated with 300 nm thermal silicon dioxide; (b) Contact pads (5 nm Ti/45 nm Au) were fabricated on top of the graphene layer by using electron-beam lithography and metal evaporation; (c) Two narrow (80 nm) grooves were patterned between Ti/Au electrodes using electron beam lithography; (d) The SLG between Ti/Au electrodes was patterned into a notched ribbon with two extra-narrow (80 nm) grooves by oxygen plasma etching; (e) The feedback-controlled electroburning process was performed; (f) One nano-gap was generated in the graphene structure located between two prepatterned grooves.

substrate to a SiO_2/Si substrate using the electrolytic bubbling method (Figure 1a).^[41] Contact pads (5 nm Ti/45 nm Au) were fabricated on top of the graphene layer by using electron-beam lithography and metal evaporation (Figure 1b). Then the SLG between Ti/Au electrodes was patterned into a notched ribbon with two extra-narrow (80 nm) grooves using e-beam lithography and oxygen plasma etching (Figs. 1c and d). The distance between Ti/Au electrodes was set to be 1 μm and the width of the graphene between grooves was 2 μm (Figure 2b). The initial low-bias resistances of the as-prepared devices were in the range from 300 Ω to 2 $\text{K}\Omega$ (See Figure S1 in the Supporting Information). We generated nano-gaps in the graphene structures using the feedback-controlled electroburning process (Figures 1e and f), which was performed at room temperature in air.

Figure 2a is a typical current-voltage (I - V) curve recorded during the feedback-controlled electroburning process. During the first few ramps, the I - V characteristics was nonlinear likely due to the removal of contaminants adsorbed on the SLG by the current annealing as reported previously.^[23,27,48] Afterward, the current started to decrease at 2.8 V, indicating the first electroburning event. Then the feedback program swept the voltage back by 20% and another voltage ramp started. With the evolution of the electroburning process, the conductance decreased successively and the power needed to trigger the electroburning also decreased. Note that our electroburning process could generate a nano-gap in one minute benefitted from a high ramping-up rate and only 20% sweeping back of the applied bias in every cycle. This is much faster than the electromigration process performed in gold nanowires, which can be as long as several hours.^[5,49] The consuming time is significant in practice when creating graphene nano-gaps in large numbers.

Using our structure and program, we not only shortened the consuming time of individual nano-gaps, but also improved the yield. Table 1 shows the statistical results of nano-gaps that we fabricated. We prepared three batches of samples and the numbers of devices are respectively 96, 189 and 94. For each device, we used our feedback-controlled electroburning program to fabricate a nano-gap. The yields are quite high, which are 98%, 98% and 97%, respectively. Therefore, the overall yield is as high as 97%. Considering the low probability of interlinking nano-gaps with single molecules, high fabrication yield of nano-gaps is critical.

To characterize the gap geometry, we took SEM images of several devices after electroburning. Figure 2b shows a representative nano-gap in the graphene structure. The gap is precisely located between two prepatterned grooves, which is an evidence of a precise control over the gap position. Benefitting from the extra-narrow groove size (80 nm), the transition from the grooves to the gap is rather smooth. The purpose of this design is to keep the size of the graphene near the gap as large as possible, so that the effects of edge defects and the quantum confinement can be minimized. Since the gap size is beyond the resolution of SEM, we cannot directly obtain an accurate gap size from the SEM characterization.

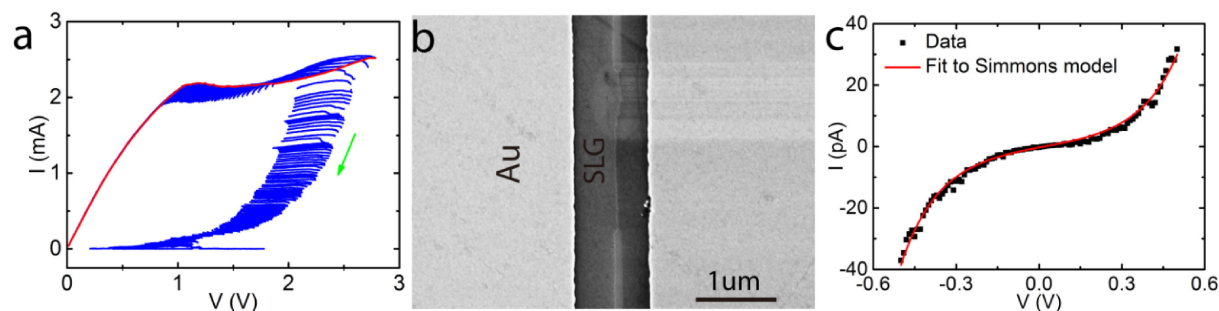


Figure 2. Fabrication of nano-gaps in graphene structures. (a) Current-voltage traces recorded during the feedback-controlled electroburning process. The I - V trace of the first cycle is in red. (b) SEM image of the graphene nano-gap. (c) Typical current-voltage data (black dotted line) of a SLG nano-gap fitted with the Simmons model for tunneling (red line). Fitting parameters: gap size $d = 1.91 \pm 0.02$ nm, barrier heights $\Phi_L = 0.59 \pm 0.01$ eV and $\Phi_R = 0.57 \pm 0.01$ eV.

Table 1. Statistical results of fabricated devices.				
	Devices fabricated	Controllably EB	Molecule connected	Survived two weeks
1st batch	96	94(98%)	5(5%)	-
2nd batch	189	185(98%)	29(16%)	11
3rd batch	97	94(97%)	25(27%)	17

One indirect way to estimate the gap size is by measuring the tunneling current through the nano-gap. Figure 2c shows a typical tunneling current as a function of the applied voltage of a graphene nano-gap fabricated by electroburning. The current is in picoampere range when the voltage is varied from -0.5 V to 0.5 V. The nonlinear I - V data can be perfectly fitted with the Simmons tunneling model (See Eq. (S1) in the Supporting Information),^[50] as shown by the red curve. Setting the tunneling cross sectional area A as 5 nm^2 , we extract a tunneling gap distance of 1.91 ± 0.02 nm and barrier heights of $\Phi_L = 0.59 \pm 0.01$ eV and $\Phi_R = 0.57 \pm 0.01$ eV. The barrier heights are comparable to that reported previously.^[20,24]

The tunneling current curve could be nicely repeated by sweeping the voltage many times, indicating that our SLG nano-gaps were stable (See Figure S2a in the Supporting Information). Moreover, we did not observe any gate-dependence of the conductance at a fixed bias voltage (See Figure S2b in the Supporting Information). Because we conducted the

electroburning process in air and the local temperature was also very high during the course of electroburning, some carbon atoms at the edges of graphene nano-electrodes were expected to be oxidized to carboxyl groups.^[51,28] These carboxyl groups can react with amine groups that molecules have on both ends.^[28,39] In summary, the graphene electrodes have several attracting features including the nanometer separation, edges decorated with carboxyl groups, room-temperature stability and the absence of gate-dependence. These features make the graphene nano-gaps suitable for constructing single-molecule devices.

As a demonstration, we used DAHP molecules to bridge the as-prepared graphene nano-gaps. The amino groups at the two ends of the DAHP molecule would react with the carboxyl groups at the edges of graphene electrodes forming graphene-hexaphenyl-graphene (GHG) junctions connected through amide groups at the two molecule-electrode interfaces, as schematically shown in Figure 3a. A significant advantage of

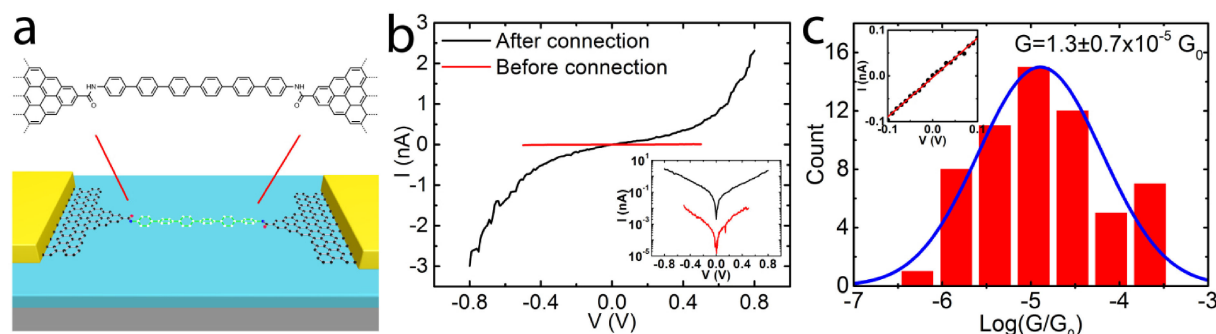


Figure 3. Electronic measurements of graphene-hexaphenyl-graphene (GHG) devices. (a) Schematic of a single-molecule device made from a hexaphenyl molecule covalently interlinked to SLG electrodes. (b) Typical current-voltage curves before (red line) and after (black line) hexaphenyl molecule connection. Inset: the same current-voltage curve plotted in a semi-logarithmic scale. (c) Low-bias conductance histogram of GHG devices. The most probable conductance value determined from the Gaussian fitting (blue line) is $(1.3 \pm 0.7) \times 10^{-5} G_0$. The insert shows a typical current-voltage curve of the GHG device in the low-bias region (black dotted line) and the least-square linear fitting (red line).

graphene electrodes is that the I - V curves before and after molecule connection can be compared directly. A distinct current increase may indicate that one or few molecules have interlinked the nano-gaps. Figure 3b shows such a comparison of a representative device before (red line) and after (black line) DAHP molecule connection. As we can see from the inset of Figure 3b plotted in a semi-logarithmic scale, an increase in the tunneling current over one order of magnitude was observed. We fabricated 373 nanogaps, out of which 59 devices showed distinct current increase after the connection of DAHP molecules. As listed in Table 1, the yield of molecular devices is up to 27%. Due to the uncontrollable atomic structures of edges of the graphene nano-electrodes and the varieties of the molecule-electrode interfacial configurations, the measured I - V curves were qualitatively similar but quantitatively different. The current always increases linearly at low bias and nonlinearly at high bias.

The low-bias conductance can be extracted from the least-square linear fitting to the I - V data in the bias range from -0.1 V to 0.1 V. The low-bias conductance histogram of 59 devices is shown in Figure 3c, which can be fitted with a Gaussian distribution. The most probable conductance value is determined to be $(1.3 \pm 0.7) \times 10^{-5} G_0$ from the Gaussian fitting (blue line in Figure 3c), where $G_0 = 2e^2/h$ is the quantum of conductance.

We can get more insights into the electronic transport properties by looking at the transition voltage spectroscopy (TVS).^[52] Figure 4a shows the Fowler-Nordheim (F-N) plots of the I - V curve (black line) shown in Figure 3b. Two obvious inflections marked with blue arrows appear in the F-N plots at the biases of $+0.46$ V and -0.44 V. As shown in Figure 4b, the statistical results of the measured transition voltages of all these 59 devices show that the most probable transition voltages at positive and negative polarities are 0.36 ± 0.14 V, and -0.38 ± 0.14 V, respectively. TVS analysis provides direct information about the energy level alignment and the coupling symmetry at the two molecule-electrode interfaces. The almost same absolute values (~ 0.4 V) of the measured transition voltages for both bias polarities indicate that the hexaphenyl molecule binds nearly symmetrically to the two graphene electrodes, and that a conducting molecular orbital centering at ~ 0.2 eV above or below the Fermi level of the graphene electrodes dominates the electronic transport.

Device stability remains one of the great challenges in the field of molecular electronics.^[17-20] The strong covalent structure of graphene promises stable electrodes at room temperature. Combined with the covalent amide linkages, our GHG single-molecule devices are expected to be stable at room temperature. This is an advantage over those constructed with metal electrodes. To test the stability of our single-molecule devices, we measured the I - V curves of the same device at different times. Figure 5 shows the I - V curves for the same GHG single-molecule device measured immediately after connection (blue line), two weeks (red line), and four weeks (green line). It is worth noting that no significant changes were observed in the I - V curves. This device was kept at room temperature in vacuum between two consecutive measurements. Statistically,

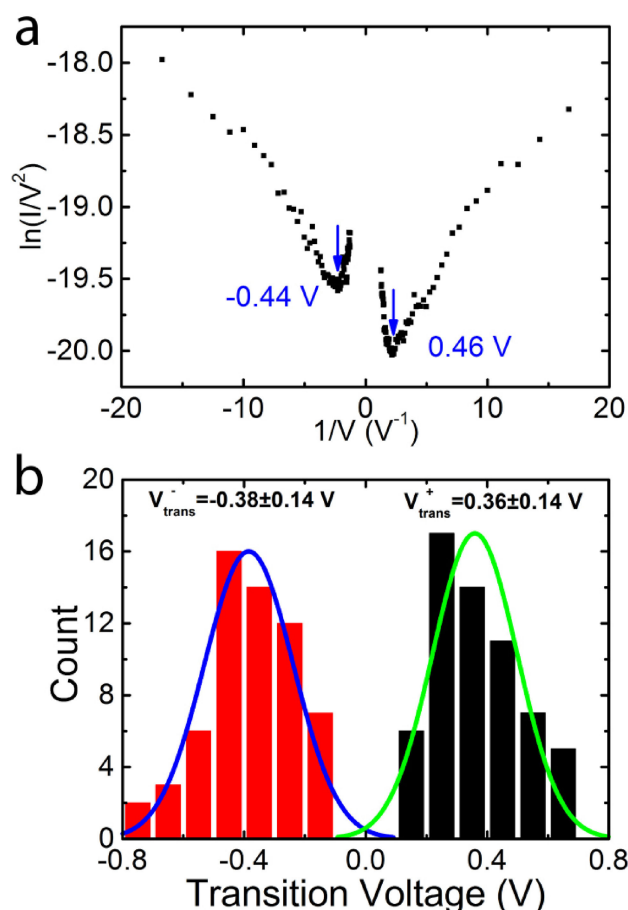


Figure 4. (a) F-N plot of a typical current-voltage curve of a GHG device. The transition voltages for positive polarity ($+0.46$ V) and negative polarity (-0.44 V) are labelled by blue arrows. (b) The statistical histogram of transition voltages. The most probable values determined from Gaussian fitting are 0.36 ± 0.14 V and -0.38 ± 0.14 V, respectively.

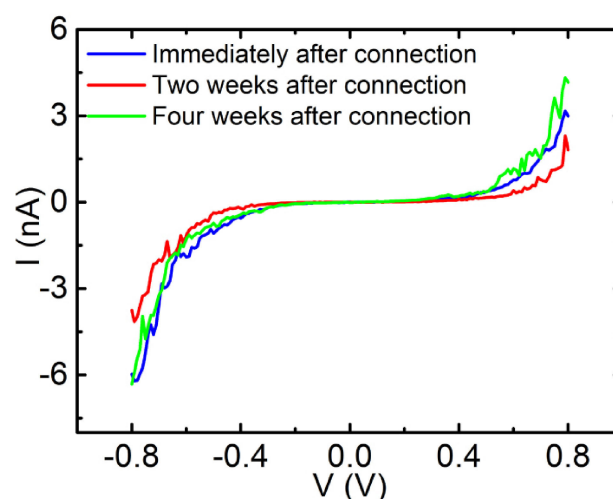


Figure 5. Current-voltage characteristics for the same GHG single-molecule device measured immediately after connection (blue line), two weeks (red line) and four weeks (green line). No significant changes were observed in the current.

more than 52% of the devices fabricated in the second and third batches could remain stable for two weeks even after several times of high bias (~ 1 V) electrical measurements (See Table 1). Because only 5 devices were successfully fabricated in the first batch, we did not test their stabilities.

To obtain a deeper understanding on the conduction mechanism of these GHG single-molecule devices, we theoretically investigated the electronic transport properties of GHG single-molecule junctions employing the NEGF + DFT approach. Figure 6a shows the optimized atomic structure of one hexaphenyl molecule bonded covalently via amide linker groups to two semi-infinite graphene electrodes with pyridinic-N doped zigzag edges. Considering that pristine graphene is a zero-gap semiconductor and that the graphene electrodes in our devices exhibit n-type transport behavior (See Figure S1 in the supporting information), we use nitrogen-doped graphene as the electrodes. More importantly, the nitrogen dopants have been proved to downshift the Dirac point of the graphene electrodes and markedly increase the density of states (DOS) around the Fermi level (E_F), but affecting marginally the alignment of frontier molecular orbitals relative to E_F .^[53] Here the graphene electrodes are doped with nitrogen atoms at a concentration level of 3.6%, which means that one carbon atom is substituted with nitrogen in a rectangle graphene cell containing 28 atoms (Figure 6a). It should be noted that, besides the zigzag edge of the graphene electrodes in our junction model, armchair and chiral edges may also exist in our fabricated GHG single-molecule devices. Because zigzag, armchair and chiral edges have different electronic properties,^[54,55] the I - V characteristics of GHG junctions with different graphene edges may also vary quantitatively.

In Figure 6b we present the computed equilibrium transmission spectrum of the GHG single-molecule junction. The transmission coefficient at E_F is calculated to be 1.6×10^{-5} ,

which is in excellent agreement with the measured value of 1.3×10^{-5} . Eigenchannels calculated at selected transmission peaks around E_F are also given to visually determine the dominant molecular orbitals for carriers transport.^[56,57] One can notice that these eigenchannels are delocalized over the molecular backbone and extend into the graphene electrodes (Figure 6c). By comparing these three eigenchannels with the lowest unoccupied molecular orbital (LUMO), the highest occupied molecular orbital (HOMO) and HOMO-1 of the isolated hexaphenyl molecule with amide groups at the two ends (see Figure S4 in the Supporting Information), we can find that the transmission peaks located at -0.24 eV and -0.43 eV are respectively dominated by the HOMO and HOMO-1 orbitals of hexaphenyl, and that the tail of the HOMO-dominated peak extends above E_F and thus determines the transmission around E_F . In contrast, the LUMO-dominated transmission peak is well above E_F and positioned at 2.25 eV. Interestingly, a small sharp transmission peak appears at -0.62 eV and the eigenchannel analysis reveals that it exhibits no distinct characters of molecular orbitals of the gas-phase hexaphenyl molecule with amide groups at the two ends. This new state is predominately localized at the amide linker and stabilized by the presence of the well-known edge states of the zigzag-terminated graphene (See Figure S5 in the Supporting Information). On the basis of the appearance of the strongly localized interface state, we speculate that hexaphenyl interacts strongly with the graphene electrodes through the amide linker groups and forms a new conducting channel with the edge states of the graphene electrodes.

Finally, we calculate the I - V characteristics and the corresponding F-N plot to clarify the role of frontier molecular orbitals of hexaphenyl in the TVS of the GHG single-molecule junctions (see Figure 6d). As we can see, the electric current increases linearly at low bias but then increases rapidly after the

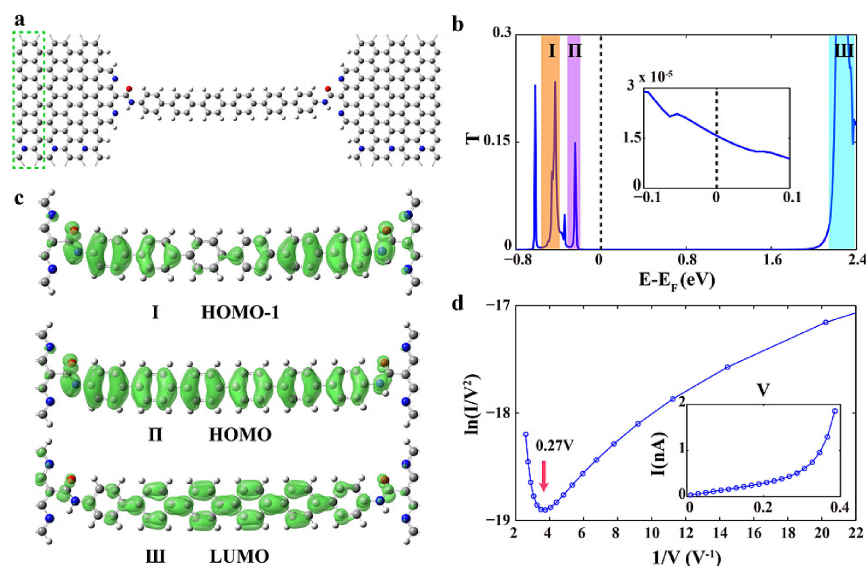


Figure 6. Theoretic calculations of the atomic structure and electronic transport properties. (a) The optimized atomic structure of a GHG junction; (b) The equilibrium transmission spectrum, the inset is a zoom-in graph on the transmission around E_F ; (c) Eigenchannels calculated at selected peak positions; (d) The F-N plot of the GHG molecular junction, the inset shows the I - V curve in a linear scale.

bias exceeds 0.2 V. Correspondingly, a well-defined minimum appears in the F–N plot and the transition voltage is determined to be 0.27 V, which is very close to the measured value (0.4 V). Because the HOMO-dominated transmission peak determines the electric current within the bias window of ± 0.4 V due to the symmetric junction structure, we can unambiguously conclude that the transition voltage is dictated by the HOMO and the GHG single-molecule junctions constructed with amide linker groups display a hole-type transport characteristic.

3. Conclusions

We have developed an optimized method for controllably fabricating nano-gaps in CVD-grown SLG using a fast-speed feedback-controlled electroburning process. In combination with pre-patterning by e-beam lithography and oxygen plasma etching, we were able to fabricate nano-gaps of ~ 2 nm with a high yield of 97%. Graphene-molecule-graphene junctions were made with hexaphenyl molecules interlinked to the graphene electrodes through amide linkages. Electronic transport measurements together with TVS analysis validated the formation of covalently bonded single-molecule devices. Our studies show that some of these molecular devices are stable for a long time at room temperature. The NEGF+DFT calculations of graphene-hexaphenyl-graphene devices agree well with the experimental measurements and specify the HOMO-dominated transport. This scalable approach opens the road to fabricate stable single-molecule devices at room temperature.

Acknowledgements

We are grateful to Prof. Hailin Peng for providing us high-quality CVD-grown SLGs. This work was financially supported by National Key R&D Program of China (2017YFA0204903, 2016YFA0201901) and the National Natural Science Foundation of China (Grant Nos. 21573014, 61671021 and 61621061).

Conflict of Interest

The authors declare no conflict of interest.

Keywords: single-molecule junctions · graphene electrode · feedback-controlled electroburning · covalent coupling · room-temperature stability

- [1] A. Nitzan, M. A. Ratner, *Science* **2003**, *300*, 1384–1389.
- [2] E. Lörtscher, *Nat. Nanotechnol.* **2013**, *8*, 381–384.
- [3] T. A. Su, M. Neupane, M. L. Steigerwald, L. Venkataraman, C. Nuckolls, *Nat. Rev. Mater.* **2016**, *1*, 16002.
- [4] M. A. Reed, C. Zhou, C. J. Muller, T. P. Burgin, J. M. Tour, *Science* **1997**, *278*, 252–254.

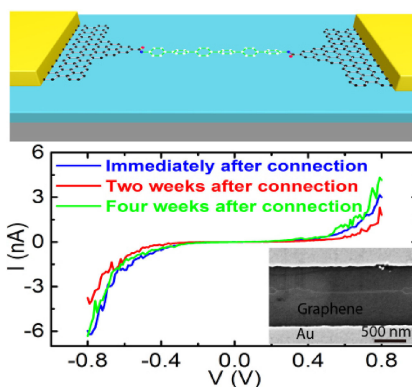
- [5] H. Park, A. K. Lim, A. P. Alivisatos, J. Park, P. L. McEuen, *Appl. Phys. Lett.* **1999**, *75*, 301–303.
- [6] X. D. Cui, A. Primak, X. Zarate, J. Tomfohr, O. F. Sankey, A. L. Moore, S. M. Lindsay, *Science* **2001**, *294*, 571–574.
- [7] B. Xu, N. J. Tao, *Science* **2003**, *301*, 1221–1223.
- [8] E. Lörtscher, B. Gotsmann, Y. Lee, L. Yu, C. Rettner, H. Riel, *ACS Nano* **2012**, *6*, 4931–4939.
- [9] B. Capozzi, J. Xia, O. Adak, E. J. Dell, Z. F. Liu, J. C. Taylor, L. Venkataraman, *Nat. Nanotechnol.* **2015**, *10*, 522.
- [10] H. Park, J. Park, A. K. Lim, E. H. Anderson, A. P. Alivisatos, P. L. McEuen, *Nature* **2000**, *407*, 57.
- [11] S. Kubatkin, A. Danilov, M. Hjort, J. Cornil, J. L. Brédas, N. Stuhr-Hansen, T. Bjørnholm, *Nature* **2003**, *425*, 698–701.
- [12] H. Song, Y. Kim, Y. H. Jang, H. Jeong, M. A. Reed, T. Lee, *Nature* **2009**, *462*, 1039–1043.
- [13] J. Guan, C. Jia, Y. Li, Z. Liu, J. Wang, Z. Yang, X. Guo, *Sci. Adv.* **2018**, *4*, eaar2177.
- [14] C. Zhou, X. Li, Z. Gong, C. Jia, Y. Lin, C. Gu, G. He, Y. Zhong, J. Yang, X. Guo, *Nat. Commun.* **2018**, *9*, 807.
- [15] A. S. Blum, J. G. Kushmerick, D. P. Long, C. H. Patterson, J. C. Yang, J. C. Henderson, B. R. Ratna, *Nat. Mater.* **2005**, *4*, 167–172.
- [16] C. Jia, A. Migliore, N. Xin, S. Huang, J. Wang, Q. Yang, Z. Liu, *Science* **2016**, *352*, 1443–1445.
- [17] L. Sun, Y. A. Diaz-Fernandez, T. A. Gschneidtner, F. Westerlund, S. Lara-Avila, K. Moth-Poulsen, *Chem. Soc. Rev.* **2014**, *43*, 7378–7411.
- [18] M. L. Perrin, E. Burzurí, H. S. J. van der Zant, *Chem. Soc. Rev.* **2015**, *44*, 902–919.
- [19] R. M. Metzger, *Chem. Rev.* **2015**, *115*, 5056–5115.
- [20] D. Xiang, X. Wang, C. Jia, T. Lee, X. Guo, *Chem. Rev.* **2016**, *116*, 4318–4440.
- [21] D. R. Strachan, D. E. Smith, M. D. Fischbein, D. E. Johnston, B. S. Guiton, M. Drndić, A. T. Johnson, *Nano Lett.* **2006**, *6*, 441–444.
- [22] K. O'Neill, E. A. Osorio, H. S. J. van der Zant, *Appl. Phys. Lett.* **2007**, *90*, 133109.
- [23] F. Prins, A. Barreiro, J. W. Ruitenbergh, J. S. Seldenthuis, N. Aliaga-Alcalde, L. M. Vandersypen, H. S. J. van der Zant, *Nano Lett.* **2011**, *11*, 4607–4611.
- [24] E. Burzurí, F. Prins, H. S. J. van der Zant, *Graphene* **2012**, *1*, 26–29.
- [25] C. Jia, B. Ma, N. Xin, X. Guo, *Acc. Chem. Res.* **2015**, *48*, 2565–2575.
- [26] M. L. Trouwborst, S. J. Van Der Molen, B. J. Van Wees, *J. Appl. Phys.* **2006**, *99*, 114316.
- [27] C. S. Lau, J. A. Mol, J. H. Warner, G. A. D. Briggs, *Phys. Chem. Chem. Phys.* **2014**, *16*, 20398–20401.
- [28] Y. Cao, S. Dong, S. Liu, L. He, L. Gan, X. Yu, X. Guo, *Angew. Chem. Int. Ed.* **2012**, *51*, 12228–12232.
- [29] Y. Cao, S. Dong, S. Liu, Z. Liu, X. Guo, *Angew. Chem. Int. Ed.* **2013**, *52*, 3906–3910.
- [30] C. Nef, L. Pósa, P. Makk, W. Fu, A. Halbritter, C. Schönenberger, M. Calame, *Nanoscale* **2014**, *6*, 7249–7254.
- [31] J. O. Island, A. Holovchenko, M. Koole, P. F. A. Alkemade, M. Menelaou, N. Aliaga-Alcalde, H. S. J. van der Zant, *J. Phys. Condens. Matter* **2014**, *26*, 474205.
- [32] J. A. Mol, C. S. Lau, W. J. Lewis, H. Sadeghi, C. Roche, A. Cnossen, G. A. D. Briggs, *Nanoscale* **2015**, *7*, 13181–13185.
- [33] C. S. Lau, H. Sadeghi, G. Rogers, S. Sangtarash, P. Dallas, K. Porfyrakis, J. A. Mol, *Nano Lett.* **2015**, *16*, 170–176.
- [34] K. Ullmann, P. B. Coto, S. Leitherer, A. Molina-Ontoria, N. Martín, M. Thoss, H. B. Weber, *Nano Lett.* **2015**, *15*, 3512–3518.
- [35] E. Burzurí, J. O. Island, R. Díaz-Torres, A. Fursina, A. González-Campo, O. Roubeau, H. S. J. van der Zant, *ACS Nano* **2016**, *10*, 2521–2527.
- [36] S. Lumetti, A. Candini, C. Godfrin, F. Balestro, W. Wernsdorfer, S. Klyatskaya, M. Affronte, *Dalt. Trans.* **2016**, *45*, 16570–16574.
- [37] P. Gehring, J. K. Sowa, J. Cremers, Q. Wu, H. Sadeghi, Y. Sheng, J. A. Mol, *ACS Nano* **2017**, *11*, 5325–5331.
- [38] S. G. Sarwat, P. Gehring, G. Rodriguez Hernandez, J. H. Warner, G. A. D. Briggs, J. A. Mol, H. Bhaskaran, *Nano Lett.* **2017**, *17*, 3688–3693.
- [39] Q. Xu, G. Scuri, C. Mathewson, P. Kim, C. Nuckolls, D. Bouilly, *Nano Lett.* **2017**, *17*, 5335–5341.
- [40] X. Wang, H. Dai, *Nat. Chem.* **2010**, *2*, 661–665.
- [41] L. Gao, W. Ren, H. Xu, L. Jin, Z. Wang, T. Ma, X. Bao, *Nat. Commun.* **2012**, *3*, 699.
- [42] J. M. Soler, E. Artacho, J. D. Gale, A. García, J. Junquera, P. Ordejón, D. Sánchez-Portal, *J. Phys. Condens. Matter* **2002**, *14*, 2745–2779.
- [43] A. R. Rocha, V. M. García-Suárez, S. W. Bailey, C. J. Lambert, J. Ferrer, S. Sanvito, *Nat. Mater.* **2005**, *4*, 335–339.

- [44] A. R. Rocha, V. M. García-Suárez, S. Bailey, C. Lambert, J. Ferrer, S. Sanvito, *Phys. Rev. B* **2006**, *73*, 085414.
- [45] I. Rungger, S. Sanvito, *Phys. Rev. B* **2008**, *78*, 035407.
- [46] N. Troullier, J. L. Martins, *Phys. Rev. B* **1991**, *43*, 1993.
- [47] J. P. Perdew, K. Burke, M. Ernzerhof, *Phys. Rev. Lett.* **1996**, *77*, 3865.
- [48] J. Moser, A. Barreiro, A. Bachtold, *Appl. Phys. Lett.* **2007**, *91*, 163513.
- [49] A. Xiang, H. Li, S. Chen, S. X. Liu, S. Decurtins, M. Bai, J. Liao, *Nanoscale* **2015**, *7*, 7665–7673.
- [50] J. G. Simmons, *J. Appl. Phys.* **1963**, *34*, 1793–1803.
- [51] X. Guo, J. P. Small, J. E. Klare, Y. Wang, M. S. Purewal, I. W. Tam, J. Yan, *Science* **2006**, *311*, 356–359.
- [52] J. M. Beebe, B. Kim, C. D. Frisbie, J. G. Kushmerick, *ACS Nano* **2008**, *2*, 827–832.
- [53] Z. Jiang, H. Wang, Y. Wang, S. Sanvito, S. Hou, *J. Phys. Chem. C* **2017**, *121*, 27344–27350.
- [54] Y. W. Son, M. L. Cohen, S. G. Louie, *Phys. Rev. Lett.* **2006**, *97*, 216803
- [55] L. Sun, P. Wei, J. Wei, S. Sanvito, S. Hou, *J. Phys. Condens. Matter* **2011**, *23*, 425301
- [56] R. Li, S. Hou, J. Zhang, Z. Qian, Z. Shen, X. Zhao, *J. Chem. Phys.* **2006**, *125*, 194113.
- [57] M. Paulsson, M. Brandbyge, *Phys. Rev. B* **2007**, *76*, 115117.

Manuscript received: June 5, 2018
Accepted Article published: May 23, 2018
Version of record online: June 20, 2018

ARTICLES

Single-molecule junctions are constructed using hexaphenyl molecules interlinked to graphene electrodes through amide groups. Molecular scale nano-gaps are generated in the graphene by an optimized fast-speed feedback-controlled electroburning process. Some of the obtained molecular devices are stable for up to four weeks, highlighting the potential of graphene nano-electrodes in the fabrication of stable single-molecule devices at room temperature.



H. Sun, Z. Jiang, N. Xin, X. Guo, S. Hou*, J. Liao*

1 – 9

Efficient Fabrication of Stable Graphene-Molecule-Graphene Single-Molecule Junctions at Room Temperature

